IEEE Access
Multidisciplinary | Rapid Review | Open Access Journal

Received 28 March 2023, accepted 14 April 2023, date of publication 25 April 2023, date of current version 3 May 2023.

Digital Object Identifier 10.1109/ACCESS.2023.3270220

RESEARCH ARTICLE

Track Misregistration Mitigation Using CNN-Based Method on Single-Reader/Two-Track Reading BPMR Systems

KITTIPON KANKHUNTHOD, (Graduate Student Member, IEEE), AND CHANON WARISARN, (Member, IEEE)
College of Advanced Manufacturing Innovation, King Mongkut's Institute of Technology Ladkrabang, Bangkok 10520, Thailand
Corresponding author: Chanon Warisarn (chanon.wa@kmitl.ac.th)

This work was supported in part by the King Mongkut's Institute of Technology Ladkrabang Doctoral Scholarships (KDS) under Grant KDS2019/031, and in part by the King Mongkut's Institute of Technology Ladkrabang under Grant KREF046407.

ABSTRACT One of the problems that cause a decrease in the performance of the ultra-high bit-patterned magnetic recording (BPMR) system is track misregistration (TMR). Since the gap between data tracks is extremely narrow, it easily affects keeping the reader in the desired position. Therefore, this paper proposes the track misregistration mitigation included the estimation and correction techniques on single-reader/two-track reading (SRTR) BPMR using only a readback signal. The TMR estimation technique uses the convolutional neural network (CNN) to estimate the TMR level by the histograms of the readback signal enabling minimization of the complexity of the CNN structure and amount of training time. The estimated TMR levels obtained from the proposed CNN-histogram-based method will then be utilized to detect the estimated recorded bit by the CNN-based data detector. The simulation shows that our proposed system provides better TMR prediction accuracy even though the system has to face higher media noise. Furthermore, the CNN-based data detectors perform superior to the partial response maximum likelihood (PRML) based data detector, especially in strong electronic noise situations and the severe imperfection of recording media.

INDEX TERMS Bit-patterned magnetic recording (BPMR), convolutional neural network (CNN), supervised learning, track misregistration (TMR).

I. INTRODUCTION

Bit-patterned magnetic recording (BPMR) [1] is one of the future hard disk drive (HDD) technology that enables the areal density (AD) gain beyond 1.0 Terabits per square inch (Tbits/in^2) [2] where a magnetic island represents one bit of data instead of many magnetic grains in existing perpendicular magnetic recording (PMR) technology. BPMR has the advantage over the PMR which a magnetic island has more energy barrier than a magnetic grain which makes it harder to be affected by ambient energy causing the change of magnetization direction [3], which we know as superparamagnetic; therefore, an AD increasing of BPMR can be achieved. To gain higher AD; the magnetic island must be carried closer together, leading to the increase of intertrack interference (ITI) and inter-symbol interference (ISI), and the crucial problem "track misregistration (TMR)" as well, which limited the bit-error-rate (BER) performance of the BPMR system [4], [5]. Generally, the TMR effect can be controlled by a servo mechanism [6], causing the recording media to lose some areas to store the servo redundancy bits. Without losing those areas and reducing this effect, the mitigation techniques of interferences and TMR for BPMR systems were proposed. For example, S. Nabavi proposed the modified Viterbi algorithm to mitigate the ITI effect. It can deliver better BER performance compared to an original Viterbi algorithm under the system that experiences the unknown TMR [7]. Warisarn proposed TMR estimation by

The associate editor coordinating the review of this manuscript and approving it for publication was Wei Wang.

using the simple energy ratio of the readback signal on a single-reader/two-track reading (SRTR) BPMR, which corrects the effect of TMR using a proper one-dimensional (1-D) generalized partial response (GPR) target and 1-D equalizer that was pre-designed corresponding to the estimated TMR levels [8].

In our previous work, the variance ratio of readback signals from a three-reader/four-track reading BPMR system was also used to estimate the TMR level and mitigate this effect using a pair of 1-D equalizer and 2-D target together with an ITI subtraction scheme [9]. The mentioned works yield better BER performances and processes without a servo mechanism.

The use of deep neural networks (DNNs) to solve the problems of magnetic recording systems was recently proposed [10], [11], [12], [13], [14], [15]. Due to it was being composed of multiple non-linear modules, it enables learning very complex functions. In some cases, it performs comparably to surpassing human expert performance [16]. For instance, in [10], the use of the multilayer perceptron (MLP) that is one of the artificial network models was adopted to improve the performance of a partial response maximum likelihood (PRML) detector in BPMR systems. Sayyafan et al. [11] also introduced the utilization of Bahl-Cocke-Jelinek-Raviv (BCJR) and convolutional neural network (CNN) turbo-detection architecture to predict the signal-dependent media noise, which can improve the detection performance on a hard disk drive (HDD) magnetic recording based on a grain flipping probabilistic (GFP) model. Li et al. [12] introduced the three tracks detection scheme in a heat-assisted interlaced magnetic recording (HIMR) system which iteratively fed the reliable soft estimate of sidetracks to improve the 2-D neural network equalization process of the middle track, then used the BCJR detector and LDPC in data detection and error correction process. Aboutaleb et al. [13] proposed three schemes of equalization and detection for multilayer magnetic recording (MLMR) where CNN is used as an equalizer, signal separator, and data detector. Han et al. [14] proposed the detection scheme based on MLPs in an array reader BPMR system; three readback signals are utilized to estimate the TMR level by the first MLP. Then, TMR effect is corrected by the second MLP in the data detection process that uses the estimated TMR level from the first MLP to be one of the inputs. The results shew an improvement in BER performance over the conventional scheme [14].

In this paper, we present the application of a CNN for TMR mitigating, which both estimation and correction of the TMR effect are investigated on the SRTR BPMR system where the reader is positioned between two considering data tracks on staggered bit-patterned media as illustrated in Figure 1. First, we estimate the TMR level of the system by using the histograms of a readback signal via the CNN-histogram-based TMR estimator, where the optimal input size is first used to maximize the prediction accuracy, reduce the complexity, training time, and computational time of CNN.

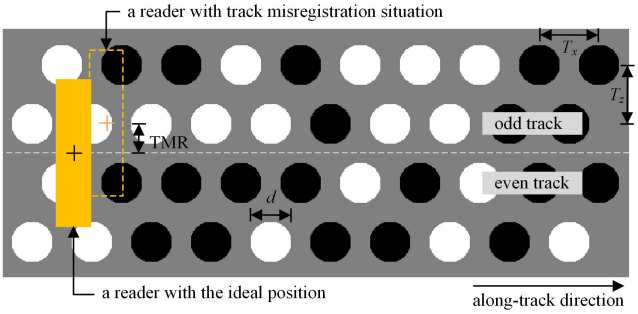

FIGURE 1. The micro-pixel staggered bit-patterned recording media and a reader with track misregistration situation under the areal density of 3.0 Tbits/in^2.

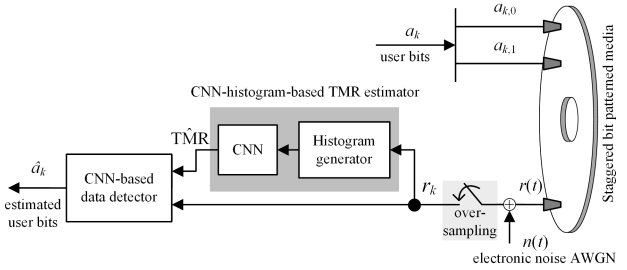

FIGURE 2. The block diagram of SRTR BPMR channel with the proposed CNN-histogram-based TMR estimator and CNN-based data detector.

Second, the estimated TMR level obtained from the proposed CNN-based estimator will then be utilized as one of the inputs in the data detection process using our proposed CNN-based data detector to perform 1-D signal processing to detect the estimated user bit sequence. Then, the BER performance of our proposed TMR mitigation method will be compared with the others.

The rest of this paper is organized as follows; Section II describes the SRTR BPMR channel model. Section III explains the proposed methods. Section IV gives the performance evaluation, and Section V concludes this work.

II. SRTR CHANNEL MODEL

This paper considers the SRTR BPMR channel model as shown in Figure 2. User bits sequence, $a_k \in \{\pm 1\}$, that is defined as an independent and identically distributed random variables (IID), is separated into two sequences that consist of odd- and even-sequences denoted by $a_{k,0}$ and $a_{k,1}$, respectively, before recording them to the medium. Note that the writing process is assumed to be perfect, the magnetization of bit-islands is always magnetized according to the recording bits.

The bit-patterned medium model is constructed by many small pixels, as illustrated in Figure 1 where the size of each pixel is set to 0.25×0.25 nm^2, and the pixel's value of the gray region is equal to 0, representing the nonmagnetic material on the medium. The black and white areas represent the magnetization direction of bit-island, which are equal to

-1, and 1 respectively. The circular magnetic islands with an average diameter $d = 10$ nm are created on the canvas. This paper considers the AD of 3.0 Tbits/in^2 where the track-pitch, T_z, and bit-period, T_x, are set to be 14.5 nm. Moreover, for obtaining more realistic SRTR BPMR channel model, the size and position fluctuations of bit islands are added and given as media noise.

The size fluctuation can be defined as the following equation,

$$\text{size fluctuation} = \frac{\sigma_d}{d}, \tag{1}$$

where d is the ideal diameter of the bit-island and σ_d is a variance of the bit-island diameter defined as a Gaussian distribution. As well as the position fluctuation is defined as follows,

$$\text{position fluctuation} = \frac{\sigma_p}{p}, \tag{2}$$

where p is the length of the bit-period, and σ_p is a variance of the distance that is compared between the center of the bit-island and the center of the ideal bit-island according to the Gaussian distribution. Note that, in this paper, the size and position fluctuations are independent and identically distributed random variables.

In the reading process, the reading position of a reader is positioned between two considering tracks, as shown in Figure 1. To obtain the readback signal, $s(x, y)$, as a function of x- and y-coordinates (in nanometer), the magnetization of each small pixel point (recording medium), $m(x, y) \in \{\pm 1\}$, was convoluted with the reader sensitivity function, $h(x, y)$, [17], [18]. Therefore, we can express the readback signal, $s(x, y)$, as follows

$$s(x, y) = \iint m(\xi, \eta) h(x - \xi, y - \eta) d\xi d\eta. \tag{3}$$

When considering the reading process in the time domain, the continuous readback signal, $s(t)$, can be constructed by $s(x, y)$ as $s(t) = s(t, l)$, where l is the center of the reader sensitivity function in across-track direction. The continuous time readback signal, $r(t)$ can be obtained by the following equation:

$$r(t) = s(t) + n(t), \tag{4}$$

where $n(t)$ is the adding additive white Gaussian noise that directly adds to the continuous time readback signal and its power spectral density is flat across the entire sampling bandwidth. Here, $n(t)$ can be calculated from

$$n(t) = \sigma \times Z, \tag{5}$$

where

$$\sigma = \frac{A}{\sqrt{10^{\text{SNR}/10}}}, \tag{6}$$

where $Z \sim \mathcal{N}(0, 1)$, Z is the random variable distributed as a standard normal distribution, with a mean equal to 0 and its standard deviation equal to 1, $A = 1$ is peak amplitude that obtained from normalizing the readback signal with the saturated level of the isolated waveform, and SNR is the signal-to-noise ratio in decibels (dB). To obtain the discrete readback signal, r_k, we use the over-sampling technique by defining $t = k \times 0.5T_x$. So, the discrete readback signal can be expressed as $r_k = r(k \times 0.5T_x)$ and it was also assumed to be the perfect synchronization. Then, the discrete readback signal is sent along two paths. The first path goes to the proposed CNN-histogram-based TMR estimator to estimate the track misregistration level. The second path leads to the CNN-based data detector to produce the estimated user bit, $\hat{a}_k$, by using the estimated TMR level, $\hat{\text{TMR}}$, to be one of the inputs of the CNN-based detector, as illustrated in Figure 2.

III. PROPOSED METHODS

A. CNN-HISTOGRAM-BASED TMR ESTIMATOR

To estimate the TMR level on the SRTR BPMR system, we propose to use the CNN performs together with the histograms of readback signal, r_k, obtained from the reading process. Figure 3 illustrates the block diagram of the CNN-histogram-based TMR estimator. First, the readback, r_k, with bit length, $N = 4{,}096$ bits for one data sector will be separated into odd- and even-sequences, which are denoted as $r_{k,0}$ and $r_{k,1}$, respectively. Each sequence of odd- and even-sequences will then be sent to the histogram generator to produce their histogram images, H'_0, and H'_1, respectively. After that, CNN predicts the TMR level from those histograms.

To construct the histogram images of readback signals, we utilize the simple histogram creation process. First, the bin- and frequency-coordinates will be obtained by setting the number of bins to be 100 where bin width, w, is calculated by $w = \left[\max(r_{k,0}) - \min(r_{k,0})\right]/100$ or $w = \left[\max(r_{k,1}) - \min(r_{k,1})\right]/100$. The frequency of each bin is obtained by counting the individual bit value of the odd- or even-readback signals within the bin's range. In our extensive study, we found that the numbers of bins are around 90 to 100 can provide the highest accuracy percentage; however, the histogram bin size of 100 yields the lowest root mean square error (RMSE) compared between the target TMR and estimated TMR levels. Therefore, we have fixed it to be 100 for this work. Second, we construct the histogram images of each readback signal by creating a blank image (where every pixel's value = 0), the number of rows and columns are set to be 250 and 100 pixels, respectively, and the number of pixel's values of each column will be replaced by 1 from the bottom of the image according to the frequency of the bin to obtain the full-size histogram, H_0 and H_1, as shown in Figure 3. Before sending the histograms to the CNN for predicting the TMR level, the histograms will be first resized into squares of $n \times n$ pixels by using Bicubic interpolation technique [19]. This resizing process aims to reduce the number of inputs and the computational complexity (number of addition and multiplication) of CNN in terms of overall feed-forward operation by down-sampling histogram images leaving only important features of the image that the optimal

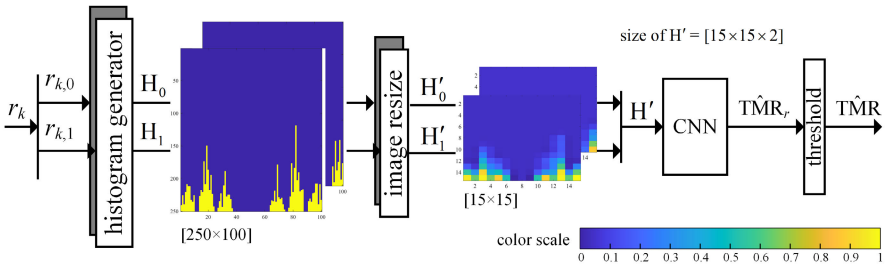

FIGURE 3. The block diagram of the CNN-histogram-based TMR estimator.

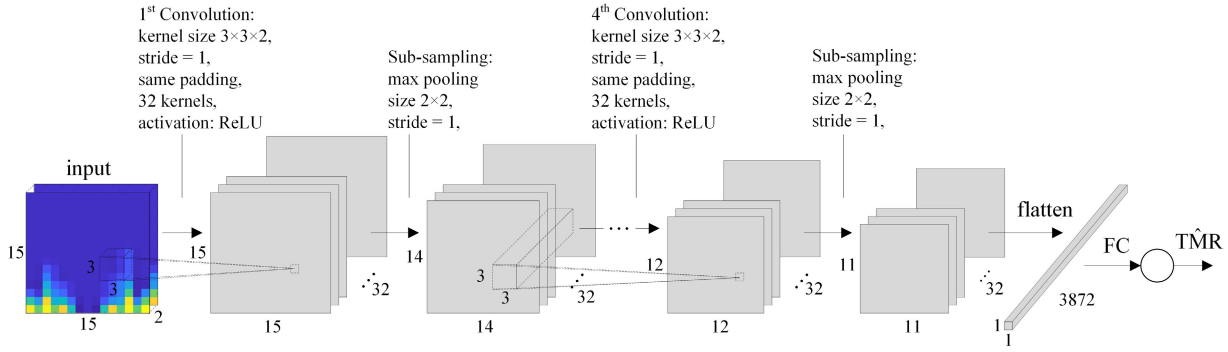

FIGURE 4. The structure of CNN on the CNN-histogram-based TMR estimator.

size can improve the estimation efficiency. The optimal input size will be discussed later in this section.

The structure of CNN consists of an image input layer, four convolutional layers, and a fully-connected layer with an output neuron, as illustrated in Figure 4; the input layer receives histograms H'_0 and H'_1, which are generated from odd- and even- readback signals. These received histograms are combined into a single histogram image, H', that consists of two channels. The convolutional layers extract the feature maps from the histogram image by 32 kernels, where the size of each kernel is set to be $3 \times 3 \times 2$. The rectified linear unit (ReLU) given as

$$f(x) = \begin{cases} 0 & \text{for } x < 0 \\ x & \text{for } x \geq 0 \end{cases}, \tag{7}$$

is used as the activation function of each convolutional layer. The max-pooling with a kernel size of 2×2 is used in the sub-sampling process after each convolutional layer. The output of the last convolutional layer will be flattened before being sent to the fully connected layer for estimating the TMR level. The CNN has 32,225 learnable parameters in total. Note that the structure of the CNN was obtained from the trial-and-error method based on fixed training data set.

In the training process, the estimated TMR value of the system is denoted by $\hat{TMR}_r$ where $\hat{TMR}_r \in \mathbb{R}$, is calculated using regression at the output neuron, and the half-mean-squared error is used as a loss function. The identity function, $f(x) = x$, is the activation function of the output neuron, where x is the function's input. The Adam (adaptative moment estimation) algorithm [20] is used to update the weights and biases of the network, the minibatch size is set to be 32, the number of training epochs and initial learning rate are set to be 80 and 0.0001, respectively. After that, the $\hat{TMR}_r$ will be passed to the multi-level threshold function to obtain the estimated TMR level, $\hat{TMR}$, according to the target of the TMR level that appears in the system.

The training data set consists of 5,200 readback signals that were generated from the SRTR BPMR channel model as mentioned in Section III under the AD of 3.0 Tbits/in^2 where the media noise is set to be 0%, at various SNRs i.e., SNR = 10, 15, 20, and 25 dB and TMR levels (−3.0 to 3.0 nm step up by 0.5 nm interval). The SNR is defined by following

$$\text{SNR} = 20\log_{10}(A/\sigma), \tag{8}$$

where σ is the standard deviation of electronic noise as defined in (6).

To optimize the input size to CNN (H'_0 and H'_1), we varied the input size of the histogram image between 5×5 to 40×40 pixels via the image resizing process, as illustrated in Figure 3, before sending it to CNN to predicting the TMR level. The stem graphs comparison between the input size to the CNN, validation accuracy, RMSE of prediction, and the computational complexity are used to evaluate the prediction performance of each input size as shown in Figure 5. Regarding accuracy, some input sizes give 100% prediction; however, the size of 15×15 pixels provides the minimum RMSE and relatively low computational complexity compared with the others. As a result, the total number of inputs

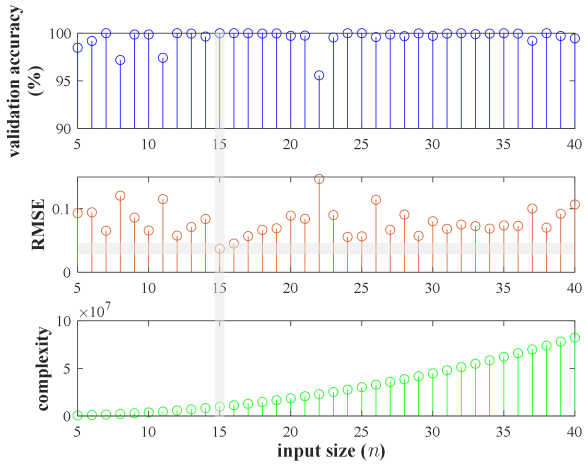

FIGURE 5. The input size of histogram image vs. validation accuracy percentage, RMSE, and computational complexity.

TABLE 1. Number of CNN layer variation of CNN-Histogram-based TMR estimator with input size $n = 15 \times 15$ pixels.

No. of CNN layer	RMSE	Accuracy percentage
1	0.1168	98.3846
2	0.0986	99.5000
3	0.0690	100.0000
4	0.0370	100.0000
5	0.0475	100.0000
6	0.0570	100.0000
7	0.0639	100.0000
8	0.0793	100.0000
9	0.0863	99.6346

to the CNN is equal to $15 \times 15 \times 2 = 450$ instead of using full-size histograms, which are equal to $250 \times 100 \times 2 = 50{,}000$. That means the input size can be reduced around 99%. So, we choose a 15×15 pixels image size for the TMR predicting process in this study. To ensure that the proposed CNN-Histogram-based TMR estimator's structure already reaches the optimal structure, we further investigate the number of CNN layer variations as shown in Table 1. The investigated results show that 3 to 8 CNN layers can yield a 100 accuracy percentage of TMR estimation. However, the number of CNN layers that is equal to 4 can provide the lowest RMSE. Therefore, we have selected this CNN structure for studying through this work.

B. CNN-BASED DATA DETECTOR

In TMR effect correction under the SRTR BPMR system, in this work, we also proposed to use the CNN-based data detector to detect the estimated user bits, $\hat{a}_k$, and correct the TMR effect instead of a conventional detector-based PRML detector [21], which consists of group detection and sliding window detection schemes.

1) GROUP DETECTION SCHEME

The first scheme is the group detection scheme. The proposed CNN-based data detector receives a group of readback

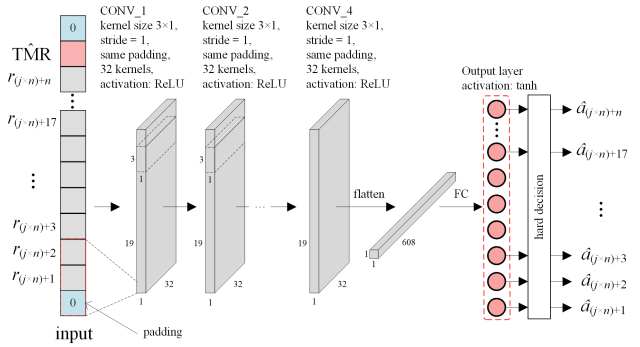

FIGURE 6. The structure of CNN-based data detector with group detection scheme.

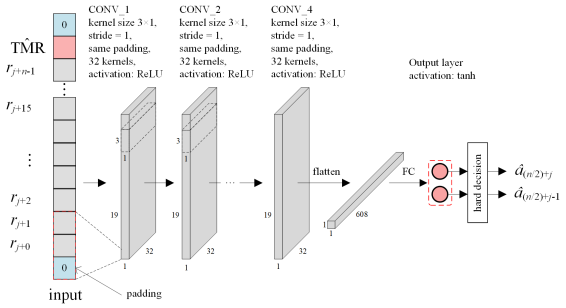

FIGURE 7. The structure of CNN-based data detector with sliding window detection scheme.

signals and estimated TMR level, $\hat{\text{TMR}}$, obtained from the Histogram-CNN-based TMR estimator as one of the inputs to produce the group of estimated user bits expressed as $\hat{a}_{(j\times n)+1}$, $\hat{a}_{(j\times n)+2}$, …, $\hat{a}_{(j\times n)+n}$ as shown in Figure 6. The group of readback signal consists of $r_{(j\times n)+1}$, $r_{(j\times n)+2}$, …, $r_{(j\times n)+n}$ which is separated from readback signal, r_k, where n is the number of bits in each group, and j, is the group's number that can be expressed as follow

$$j \in \begin{cases} 0, 1, 2, \ldots, \text{floor}(N/n) & \text{for } n \nmid N \\ 0, 1, 2, \ldots, N/n - 1 & \text{for } n \mid N \end{cases} \quad (9)$$

where $N = 4{,}096$ is the bit length of readback signal, the symbol "$|$" and "$\nmid$" denote divisible and indivisible, respectively.

As illustrated in Figure 6, the structure of a CNN-based data detector consists of an input layer, four convolutional layers, and a fully connected layer with n output neurons. As the input layer, it receives a vector input, which has a size of $n + 1$. Each convolutional layer uses 32 kernels with the size of 3×1 to extract feature maps from the input vector. The ReLU is used as an activation function. Zero padding is used in every convolutional layer to prevent output size reduction and loss of some crucial input information. The last convolutional layer's output will be flattened to be the input of a fully connected layer before calculating output to the n output neurons of the output layer, where each neuron uses the

hyperbolic tangent function as an activation function, given as

$$\tanh(x) = \frac{e^{x} - e^{-x}}{e^{x} + e^{-x}}. \tag{10}$$

The outputs of the output layer will be passed through a hard decision process to obtain estimated user bits.

The training of the proposed CNN-based data detector is processed in the same manner as the CNN-histogram-based TMR estimator except for the output layer's activation function and training data set, where the number of training epochs and initial learning rate are set to be 20 and 0.0001, respectively. The training data set consists of 4,680 readback signals generated at various media noise (0, 5, and 10%), SNRs (5, 10, 15, 20, 25, 30 dBs), and TMR levels (−3.0 to 3.0 nm step up by 0.5 nm interval). To optimize the number of bits in a group, n, to be an input of the CNN. First, we start from the small amount of training data set to investigate the rough performance trend. There is 25% of the training data set was selected for training the network. The number of bit in a group is varied from 4 to 30, and the overall BER performances are collected as shown in Table 2 by using the 5,200 readback signals generated under media noise 5%, SNR = 5, 10, 15, 20 dBs, and TMR = −3.0 to 3.0 nm step up by 0.5 nm interval. The results show that n values around 14 to 18 can deliver good BER performance. Second, we increase the training data to 100% and train the model with n values between 12 to 20 to improve the BER results, as shown in Table 3. The results show that $n = 18$ provides the best BER performance, so in this paper, we decided to use this number of inputs in the CNN-based data detector with group detection scheme. After that, the total number of inputs to CNN is equal to 19 by adding one more input obtained from the TMR estimator.

2) SLIDING WINDOW DETECTION SCHEME

Furthermore, we also propose the CNN-based data detector with sliding window detection by feeding the readback signal in sliding window manner, as shown in Figure 7. The structure of CNN-based data detector with sliding window detection is the same as the CNN-based data detector with group detection scheme except for the number of outputs, which is fixed to be two outputs. The outputs consist of $\hat{a}_{(n/2)+j-1}$ and $\hat{a}_{(n/2)+j}$. The input consists of a group of readback signal, which are equal to the window size, n, and an estimated TMR level obtained from a CNN-histogram-based TMR estimator, $\hat{\text{TMR}}$. The group of readback signal consists of r_{j+0}, r_{j+1}, r_{j+2}, …, r_{j+n-1} where $j \in \{1, 3, 5, 7, 9, \ldots, (N - n + 1)\}$, $N = 4{,}096$, and $n \in \{4, 6, 8, 10, 12, \ldots, 4096\}$. We perform two-stride for the sliding window to keep the first output, $\hat{a}_{(n/2)+j-1}$, and the second output, $\hat{a}_{(n/2)+j}$ belong to the odd- and even-tracks, respectively, for convenience in model training. For example, if we consider $(n, j) = (4, 1)$, it means that the considered inputs will be $\{r_1, r_2, r_3, r_4\}$ and the detected outputs are $\{\hat{a}_2, \hat{a}_3\}$. In case $(n, j) = (6, 3)$, the inputs will become $\{r_3, r_4, r_5, r_6, r_7, r_8\}$ and the outputs should be $\{\hat{a}_5, \hat{a}_6\}$.

TABLE 2. CNN-based data detector input size variation with 25% training data (group detection scheme).

Input size (n)	BER ($\times 10^{-4}$)	Training time (minutes)
4	8.8666	638
6	2.8511	234
8	3.4748	153
10	2.2036	154
12	2.2339	117
14	1.9162	77
16	1.9922	69
18	1.7194	64
20	3.1674	55
22	3.1801	42
24	7.1078	58
26	3.6244	37
28	3.9327	43
30	7.1895	40

TABLE 3. CNN-based data detector input size variation with 100% training data (group detection scheme).

Input size (n)	BER($\times 10^{-5}$)	Training time (minutes)
12	6.078	828
14	9.628	494
16	7.416	401
18	4.581	355
20	7.699	373

TABLE 4. CNN-based data detector input size variation with 100% training data (sliding window scheme).

Input size (n)	BER ($\times 10^{-5}$)
4	117.467
6	61.976
8	28.398
10	16.320
12	32.145
14	7.464
16	4.022
18	64.032
20	49.255
22	21.195
24	40.677
26	105.136
28	20.416
30	24.1563

In the training process, we fixed the training parameters identically to the group detection scheme with 100% training data set. The BER performances are collected using the same data set as the group detection scheme. The size of the sliding window, n, is varied in the range of $\{4, 6, 8, 10, 12, \ldots, 30\}$. Table 4 shows the BER performances and size of the sliding window, which shows that the $n = 16$ is optimal for the sliding window scheme.

IV. SIMULATION RESULTS

A. TMR PREDICTION ACCURACY

To evaluate the performance of the proposed CNN-histogram-based TMR estimator, the 46,800 readback signals are fed to the TMR estimator as the testing data, which were generated under the various media noise (0, 5, and 10%), at various SNR levels (5, 10, 15, 20, 25, and 30 dBs), and

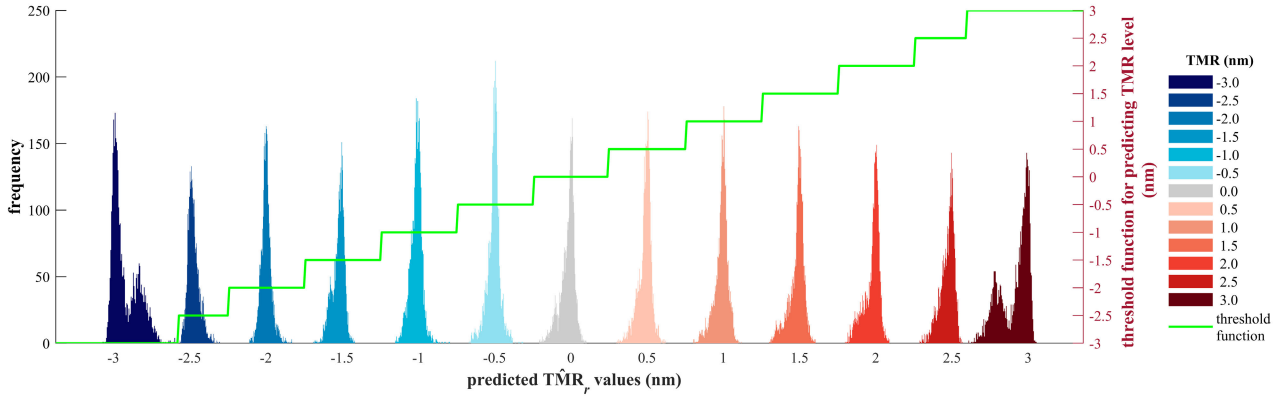

FIGURE 8. The distribution of predicted outputs from the CNN-histogram-based TMR estimator.

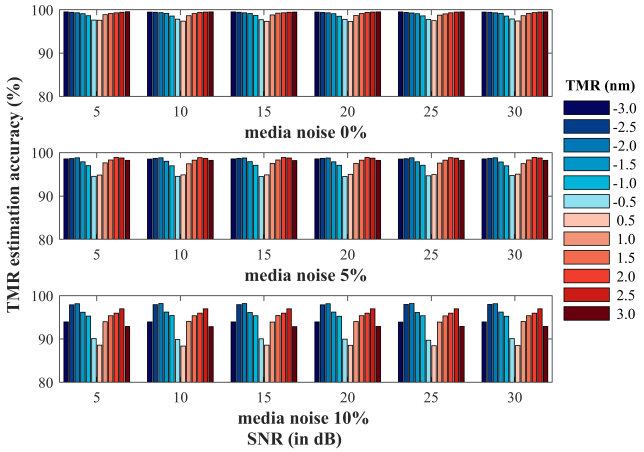

FIGURE 9. TMR estimation accuracy by proposed CNN-histogram-based TMR estimation at various SNRs under media noise 0, 5, and 10%.

various TMR levels (−3 to 3 nm, step up by 0.5 nm interval). The distribution of predicted outputs is the estimated TMR values denoted as $\hat{TMR}_r$, which can be plotted and shown in Figure 8, where each color represents the desired TMR level to which the outputs belong. The distribution plot shows that there is no overlap area between adjacent groups of outputs. Therefore, we can create a multi-step function as the classifier to decide the estimated TMR values, $\hat{TMR}_r$, to be the desired estimated TMR level, $\hat{TMR}$, according to their TMR level.

Figure 9 illustrates the accuracy percentage of TMR estimation, which is calculated by the following equation:

$$\text{accuracy}(\%) = 100 - \frac{\left|\text{TMR} - \hat{\text{TMR}}_r\right|}{\text{TMR}} \times 100, \qquad (11)$$

where TMR is the target TMR level, and $\hat{TMR}_r$ is the estimated TMR value obtained from the proposed CNN-histogram-based TMR estimator. The proposed method provides TMR estimation accuracy at various TMR and SNR levels more than 90% for media noise 0 and 5%. At a media noise of 10%, the accuracy percentage looks worse. However, all of them still provide accuracy over 88% because of the severe media noise at 10%, which is the size of bit islands and their center's positions deviate from the ideal making the CNN detector performance deteriorate. Moreover, the accuracy percentage patterns, as shown in Figure 9, also imply that the accuracy percentage is independent of electronic noises.

B. BER PERFORMANCES

We evaluate the CNN-based data detector from our proposed TMR correction schemes on a staggered SRTR BPRM system as illustrated in Figure 2 under AD of 3.0 Tbits/in^2. Figure 10 shows the BER performance of our proposed TMR correction, which consists of a CNN-histogram-based TMR estimator and CNN-based data detector with group detection scheme denoted by "Prop. system I" compared with the "System I," which is the conventional SRTR BPMR system without TMR correction where used 1-D equalizer and 1-D monic constrained GPR target designed for a non-TMR situation in the data detection process, and "System II" represents the system that uses a pair of 1-D equalizer and 1-D monic constrained GPR target designed according to each TMR level in the data detection process and detect data bits by PRML-based detector [8]. In this work, the coefficients of GPR target and equalizer in "System I" and "System II" are set to be 1×3 and 1×11 taps, respectively [8]. Since the distribution of estimated TMR values represented in Figure 8 are non-overlapped. Therefore, we assumed that in the BER collection process, the TMR estimation process provides perfect TMR estimation in order to analyze only the detection efficiency. Each point of BER performance is calculated using 819,200 randomized bits.

As mentioned above, we then compare the computational complexity per bit of each detection scheme illustrated in Table. 5 where "System I" and "System II" employ PRML-based detection that performs under the equalization and detection processes. The PRML-based detection's computational complexity will be considered under the number of equalizer coefficients and the number of addition and multiplication in each stage of 1-D Viterbi detector. While, the

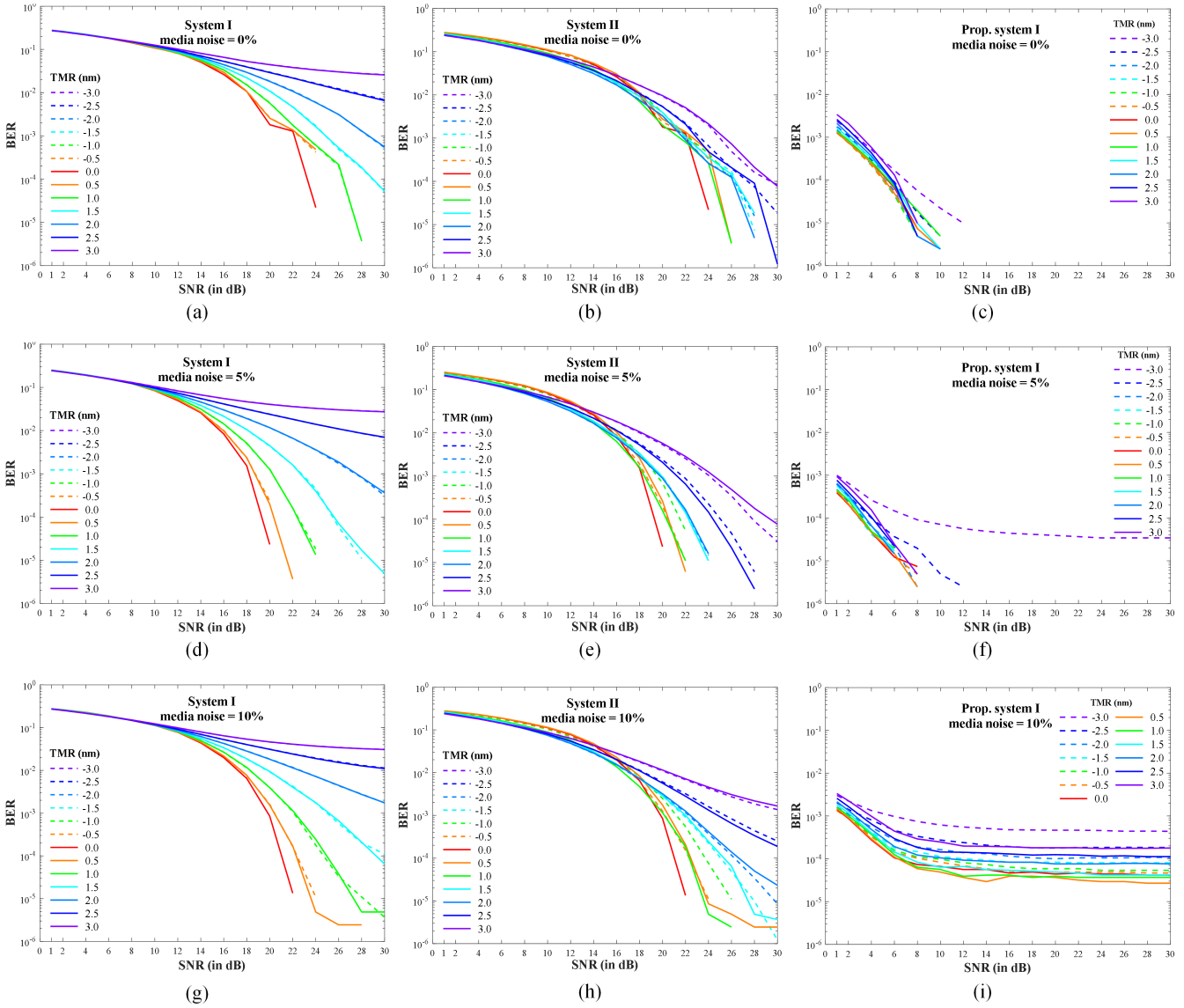

FIGURE 10. BER performances of the "System I," "System II," and "Prop. system I" at various media noise under the group detection scheme.

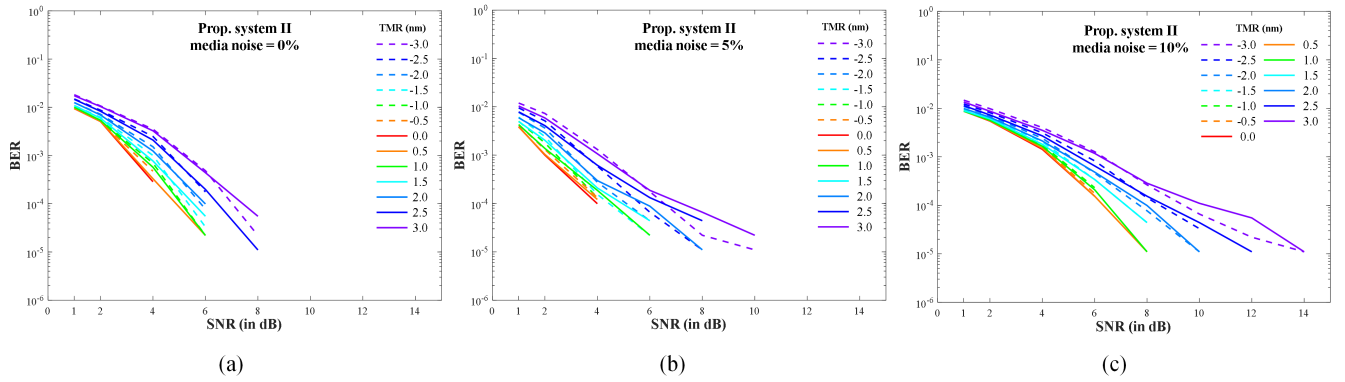

FIGURE 11. BER performances of the "Prop. system II" at various media noise under the sliding window detection scheme.

"Prop. system I" and "Prop. system II" employ CNN-based data detectors which differ in the number of inputs, outputs, and detection behavior. Here, the computation complexity of CNN can be calculated as provided in [23].

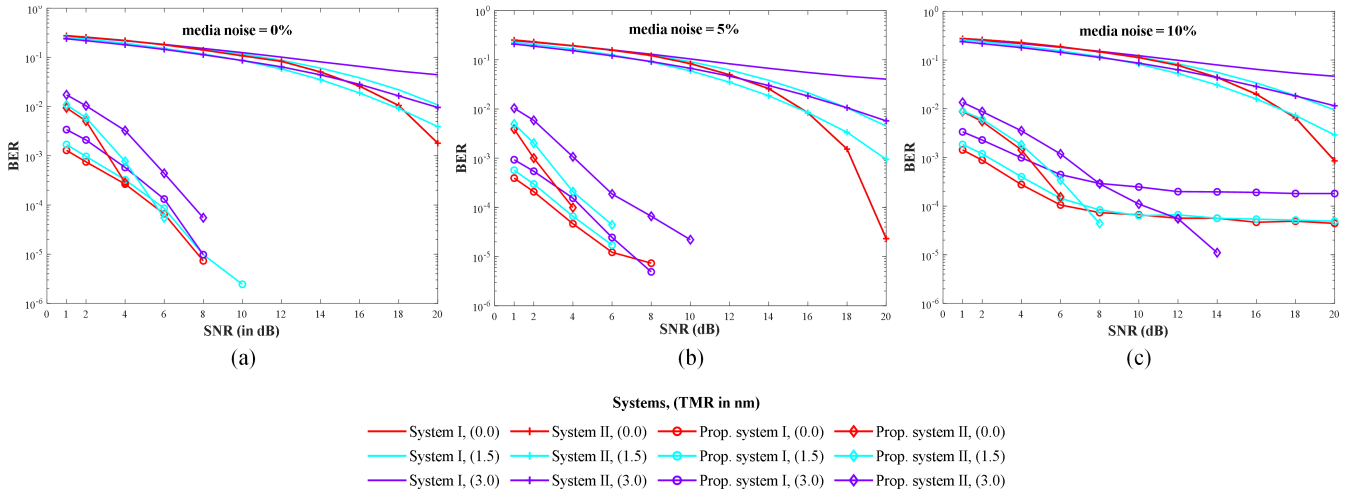

FIGURE 12. BER performance comparison at positive TMR level of all systems at various media noise, where "Prop. system I" and "Prop. system II" represent the group and sliding window detection schemes, respectively.

TABLE 5. Detection computational complexity per bit.

Detection schemes	Computational complexity per bit (addition and multiplication)		
	1-D equalization (11 tabs)	1-D Viterbi detector	Total
1. PRML-based detector (System I and System II)	21	24	$21 + 24 = 45$
2. CNN-based data detector (Group detection scheme, Prop. system I)	NaN	NaN	$19,726$
3. CNN-based data detector (Sliding window detection scheme, Prop. system II)	NaN	NaN	$149,504$

Considering Figure 10 (a), (b), and (c), where the media noise is set to be 0%, we will see that our proposed scheme can provide an outstanding BER performance than "System I" and "System II". The "Prop. system I" have 17 dBs performance gain at a target BER = 10^{-4} for TMR = 0 nm compared to other systems. At the media noise 5%, Figure 10 (d), (e), and (f), the "Prop. system I" delivers better performance than others except for TMR level -3 nm. Figure 10 (g), (h), and (i) represent all systems at media noise 10%; the proposed scheme provides lower BER than others at strong electronic noise region. Moreover, when the system suffered from the TMR effect, our proposed CNN-based data detector with group detection scheme can correct this effect effectively, as shown in Figure 10 (c) and (f) at media noise 0% and 5%. At media noise of 10%, there is a performance degradation at high SNR; however, at low SNR the BER performance is still superior to other systems. It is important to note that we can utilize the iteration detection process such as a low-density parity-check code (LDPC) [22] together with our proposed system to improve the BER performances where it has the BER performances degradation as shown in Figure 10 (i).

Figure 11 (a), (b), and (c) illustrate the BER performances of CNN-based data detector under sliding window detection scheme denoted by "Prop. system II" at media noise 0%, 5%, and 10%, respectively. Considering Figure 11 (c), the BER performances under severe media noise 10% can be improved when compared with the group detection scheme shown in Figure 10 (i), we can see from the absence of the performances degradation at low SNR region in Figure 11 (c).

The BER performance comparison at positive TMR levels between "Prop. system I," "Prop. system II," "System I," and "System II" are plotted in Figure 12 for easy evaluation. Figure 12 (a), (b), and (c) show the performances under media noise 0%, 5%, and 10%, respectively. These figures show the trend of BER performances of our proposed CNN-based data detectors (both group and sliding window detection schemes) and the other systems. As we have seen, the proposed CNN-based data detectors ("Prop. system I" and "Prop. system II") perform better than "System I" and "System II," especially at extreme electronic noise because the CNN-based data detectors are constructed from elements that can learn the signal patterns under TMR effect, and we can imply that it is able to isolate the electronic noise excellently. However, the impact of the media noise still affects its performance to some extent. We compared the "Prop. system I" and "Prop. system II" for all media noise, the group detection scheme provides lower BER than the sliding window scheme at extreme electronic noise region, but the sliding window scheme offers better BER performance under strong media noise 10% at moderate and high SNR region. Although the sliding window detection scheme can provide better performance than the group detection scheme and PRML-based detector; however, it must be invested with the cost of greater processing time and higher complexity. Note

that BER performances of "System I, (0.0)" and "System II, (0.0)" are completely overlapping each other because they use the same GPR target and 1-D equalizer's coefficient.

V. CONCLUSION

In this paper, we propose the techniques for estimation and correction of track misregistration (TMR) effect on a single-reader/two-track reading (SRTR) bit-patterned magnetic recording (BPMR) system. First, we present the convolutional neural network (CNN) histogram-based TMR estimator that uses the histograms of a readback signal to estimate the TMR level. The optimal input size of the histogram that is used to be as an input of CNN was studied for the best estimation accuracy. Second, CNN-based data detectors are also proposed to improve overall system performance, which consists of group detection and sliding window detection schemes. The estimated TMR level that was generated from the first CNN-histogram-based TMR estimator is then adopted to be one of the inputs of the CNN-based data detectors. The simulation results show that our proposed CNN-histogram-based TMR estimator can provide a high accuracy percentage. Therefore, it leads to getting better bit-error-rate performance when the CNN-based data detectors experience the severe TMR effect, position and size fluctuations, and electronic noises.

REFERENCES

[1] G. F. Hughes, "Patterned media recording systems—The potential and the problems," in *Proc. IEEE Int. Magn. Conf. (INTERMAG)*, Amsterdam, The Netherlands, Apr./May 2002, p. GA6.

[2] H. J. Richter, A. Y. Dobin, K. Gao, O. Heinonen, R. J. Van de Veerdonk, R. T. Lynch, J. Xue, D. K. Weller, P. Asselin, M. F. Erden, and R. M. Brockie, "Recording on bit-patterned media at densities of 1Tb/in^2 and beyond," in *Proc. IEEE Int. Magn. Conf. (INTERMAG)*, May 2006, p. 721.

[3] C. A. Ross, "Patterned magnetic recording media," *Annu. Rev. Mater. Res.*, vol. 31, no. 1, pp. 203–235, 2001.

[4] S. Nabavi and B. V. K. V. Kumar, "Two-dimensional generalized partial response equalizer for bit-patterned media," in *Proc. IEEE Int. Conf. Commun.*, Jun. 2007, pp. 6249–6254.

[5] S. Koonkarnkhai, C. Warisarn, and P. Kovintavewat, "A novel ITI suppression technique for coded dual-track dual-head bit-patterned magnetic recording systems," *IEEE Access*, vol. 8, pp. 153077–153086, 2020.

[6] Y.-B. Chang, D.-K. Park, N.-C. Park, and Y.-P. Park, "Prediction of track misregistration due to disk flutter in hard disk drive," *IEEE Trans. Magn.*, vol. 38, no. 2, pp. 1441–1446, Mar. 2002.

[7] S. Nabavi, B. V. K. V. Kumar, and J.-G. Zhu, "Modifying Viterbi algorithm to mitigate intertrack interference in bit-patterned media," *IEEE Trans. Magn.*, vol. 43, no. 6, pp. 2274–2276, Jun. 2007.

[8] C. Warisarn, "Mitigating the effects of track mis-registration in single-reader/two-track reading BPMR systems," *IEEE Trans. Magn.*, vol. 55, no. 7, pp. 1–6, Jul. 2019.

[9] K. Kankhunthod, C. Buajong, and C. Warisarn, "Optimal array-reader and track misregistration mitigation method in a three-reader/four-track reading bit-patterned magnetic recording system," *IEEE Magn. Lett.*, vol. 11, pp. 1–5, 2020.

[10] S. Jeong and J. Lee, "Iterative signal detection scheme using multilayer perceptron for a bit-patterned media recording system," *Appl. Sci.*, vol. 10, no. 24, p. 8819, Dec. 2020.

[11] A. Sayyafan, B. J. Belzer, K. Sivakumar, J. Shen, K. S. Chan, and A. James, "Deep neural network based media noise predictors for use in high-density magnetic recording turbo-detectors," *IEEE Trans. Magn.*, vol. 55, no. 12, pp. 1–6, Dec. 2019.

[12] Y. Li, Y. Wang, Y. Xu, L. Chen, Y. Wen, and P. Li, "Multitrack detection with 2-D iterative soft estimate aided neural network equalizer for heat-assisted interlaced magnetic recording," *IEEE Trans. Magn.*, vol. 57, no. 3, pp. 1–8, Mar. 2021.

[13] A. Aboutaleb, A. Sayyafan, K. Sivakumar, B. Belzer, S. Greaves, K. S. Chan, and R. Wood, "Deep neural network-based detection and partial response equalization for multilayer magnetic recording," *IEEE Trans. Magn.*, vol. 57, no. 3, pp. 1–12, Mar. 2021.

[14] S. Han, G. Kong, and S. Choi, "A detection scheme with TMR estimation based on multi-layer perceptrons for bit patterned media recording," *IEEE Trans. Magn.*, vol. 55, no. 7, pp. 1–4, Jul. 2019.

[15] T. Chantakit, C. Buajong, and C. Warisarn, "Long-short term memory-based application on adaptive cross-platform decoder for bit patterned magnetic recording," *IEEE Access*, vol. 8, pp. 155248–155259, 2020.

[16] Y. LeCun, Y. Bengio, and G. E. Hinton, "Deep learning," *Nature*, vol. 521, pp. 436–444, Dec. 2015.

[17] M. Yamashita, O. Hisashi, Y. Okamoto, Y. Nakamura, Y. Suzuki, K. Miura, and H. Muraoka, "Read/write channel modeling and two-dimensional neural network equalization for two-dimensional magnetic recording," *IEEE Trans. Magn.*, vol. 47, no. 10, pp. 3558–3561, Oct. 2011.

[18] Y. Okamoto, K. Ozaki, M. Yamashita, Y. Nakamura, H. Osawa, and H. Muraoka, "Performance evaluation of ITI canceller using granular medium model," *IEEE Trans. Magn.*, vol. 47, no. 10, pp. 3570–3573, Oct. 2011.

[19] R. G. Keys, "Cubic convolution interpolation for digital image processing," *IEEE Trans. Acoust., Speech, Signal Process.*, vol. ASSP-29, no. 6, pp. 1153–1160, Dec. 1981.

[20] D. P. Kingma and J. Ba, "Adam: A method for stochastic optimization," 2014, *arXiv:1412.6980*.

[21] G. D. Fisher, W. L. Abbott, J. L. Sonntag, and R. Nesin, "PRML detection boosts hard-disk drive capacity," *IEEE Spectr.*, vol. 33, no. 11, pp. 70–76, Nov. 1996.

[22] R. G. Gallager, "Low-density parity-check codes," *IRE Trans. Inf. Theory*, vol. 8, no. 1, pp. 21–28, Jan. 1962.

[23] L. Guo, "SAR image classification based on multi-feature fusion decision convolutional neural network," *IET Image Process.*, vol. 16, no. 1, pp. 1–10, Jan. 2022.

KITTIPON KANKHUNTHOD (Graduate Student Member, IEEE) received the B.Eng. degree (Hons.) in manufacturing systems from the College of Advanced Manufacturing Innovation, King Mongkut's Institute of Technology Ladkrabang (KMITL), Bangkok, Thailand, in 2017, and the M.Eng. degree in instrumentation from the Faculty of Engineering, KMITL, in 2019, where he is currently pursuing the Ph.D. degree with the College of Advanced Manufacturing Innovation.

His research interests include signal processing for data storage systems, read channel modeling, magnetic recording simulation, deep learning, and control systems.

CHANON WARISARN (Member, IEEE) received the B.Eng. degree (Hons.) in electronics engineering technology from the King Mongkut's Institute of Technology North Bangkok (KMITNB), Thailand, in 2006, and the Ph.D. degree in electrical engineering from the King Mongkut's Institute of Technology Ladkrabang (KMITL), Bangkok, Thailand, in 2011.

He is currently with the College of Advanced Manufacturing Innovation (AMI), KMITL. His current research interest includes communications and signal processing for data storage systems.